

# **Ratchet Effect on Gas Transport by Nanoporous Graphene - Significant Enhancement of Vapor Generation**

Hongru Ding<sup>1,2,#</sup>, Guilong Peng<sup>1,2,#</sup>, Dengke Ma<sup>1,2</sup>, S.W. Sharshir<sup>1,2</sup> and Nuo Yang<sup>1,2,\*</sup>

<sup>1</sup>State Key Laboratory of Coal Combustion, Huazhong University of Science and Technology (HUST), Wuhan 430074, P. R. China

<sup>2</sup>Nano Interface Center for Energy(NICE), School of Energy and Power Engineering, Huazhong University of Science and Technology (HUST), Wuhan 430074, P. R. China

# H. D. and G. P. contributed equally to this work.

Electronic mail: N.Y. ([nuo@hust.edu.cn](mailto:nuo@hust.edu.cn))

---

## **ABSTRACT**

Ratchet effect can give rise to nonzero mass flux under a zero-mean time-dependent drive. In this paper, we propose a new class of two-dimensional nano-ratchet: multilayer graphene with truncated-cone nanopores (GTCN). By performing molecular dynamics simulations, we find air molecules spontaneously transport to the small pores side of GTCN and form a remarkable pressure difference between the two sides of GTCN. The resulting pressure difference could give rise to more than 15 times enhancement of vapor generation. The number of graphene layers, the angle of the truncated-cone pores, the size of pores and the ambient temperature have significant effects on the ratchet transport. By further analysis of the force and potential profiles, we identified that the pressure difference relates to the competition between ratchet transport and diffusive transport. This work provides a novel and potential way to improve the vapor generation and proposes a guideline to produce a high performance GTCN.

**KEYWORDS:** Ratchet, thermal fluctuations, graphene membranes, pressure difference, vapor generation, evaporation

## Introduction

Water vapor generation has a broad range of applications, from power generation<sup>1-2</sup>, desalination<sup>3</sup>, water purification<sup>4</sup> to oil recovery<sup>5</sup> and so on. Whereas, the limited evaporation rate impeded the further development of those field. Over the past decades, many researches including localizing heat, using nanoparticles or thin-film and constructing vacuum have been carried out to improve vapor generation.<sup>6-12</sup> Among them, providing vacuum has proved very effective: In 2007, Nassar et al.<sup>11</sup> achieved 303% improvement of the productivity of desalinated water under vacuum of 25 kPa by using a vacuum pump; and later, Kabeel et al.<sup>12</sup> obtained an increase of 53.2% in the total daily distillation when provided vacuum with a fan. However, all of the traditional methods to create vacuum need extra energy and devices, which increases the cost and complexity of the system. Obviously, a green and simple way to create vacuum for vapor generation is in pressing need.

Interestingly, an amazing phenomenon called the ratchet effect<sup>13</sup> may provide a brand new and green approach to get vacuum. The ratchet theory, initiates from Smoluchowski in 1912<sup>14</sup>, indicates that asymmetric potentials, such as thermal gradient<sup>15-16</sup>, magnetic gradient<sup>17</sup>, chemical gradient<sup>18</sup> and electric field<sup>19-20</sup>, are able to produce net mass or energy flux under zero-average dynamic load. Asymmetric structures acting as the ratchet were also reported in recent years.<sup>21-24</sup> Additionally, Doering et al.<sup>25-27</sup> had demonstrated the existence of noise-driven ratchet, which consumes energy extracted from thermal fluctuations of the environment. Therefore, unidirectional air molecules flux can be introduced by asymmetric nanostructures, through rectifying thermal fluctuations. Then vacuum is created by harvesting only green energy.

In addition, both theoretical studies<sup>28-29</sup> and experiments<sup>30-31</sup> have proved carbon nanotubes (CNT) as fast water transporters for its regular structure and the hydrophobic nature.<sup>32</sup> With the same hydrophobic nature and similar structure, multilayer graphene

with truncated-cone nanochannel is expected to keep the fast water molecules flow rate and this will guarantee the significant reduction of energy intensity.

In view of the advance in synthesis of graphite atomic-scale channel<sup>33</sup>, the current work aims to provide a guide line for constructing the above system. We show the multilayer graphene with truncated-cone nanopores (GTCN) can spontaneously pump saturated moist air molecules from the low pressure region to the high one. We also investigated the following factors that can affect the pumping efficiency: the number of graphene layers, the aperture of the cone, the angle of the truncated-cone and the ambient temperature. Moreover, we suggest the physical mechanism of the GTCN's ratchet effect and discuss its potential to be applied in vapor generation. This may provide a new way for studying the molecular transport in asymmetric membranes and promote the vapor generation's development.

## Method

The simulation domain consists of two blocks of saturated moist air separated by GTCN (Fig. 1). The periodic boundary conditions were applied in X and Y directions and rigid walls were applied in the ends of Z direction. Truncated-cone nanopores were created by removing carbon atoms within different distance from the center of a hexagonal graphene ring. Initially, the air pressure ( $P_0$ ) of the two identical blocks is 101 kPa and the molecular ratio between  $N_2$ ,  $O_2$  and  $H_2O$  molecules is 26:8:1. Figure 1 also illustrates the physics of the ratchet effect in GTCN. The thermal fluctuations act as the rod, running back and forth. The GTCN acts as the pawl, preventing the anticlockwise rotation. Then the rotary direction of the gear is clockwise. That is the transport direction of the air atoms is leftward.

Simulations were performed with the LAMMPS package<sup>34</sup>, with a time step of 1 fs. The intermolecular interactions, essential to this study, were modeled by Lennard-Jones(LJ) potential  $V(r) = 4\epsilon[(\frac{\sigma}{r})^{12} - (\frac{\sigma}{r})^6]$  plus Coulomb potential. Two centered LJ

potential models<sup>35</sup> and rigid TIP4P<sup>36</sup> model are used for the N<sub>2</sub> and O<sub>2</sub> pairwise potential and water molecules, respectively. Long-range electrostatic forces were computed with the P<sup>3</sup>M method. For graphene, the LJ parameters were adopted from the work of Beu et al<sup>37-38</sup>. For all pairwise LJ terms, the Lorentz-Berthelot mixing rules were applied and the cutoff distance in LJ potential was set to  $2.5\sigma$ .

NEMD simulations in the NVT ensemble were used to compute the density distribution and pressure of the air, after the relaxation of the system in the NVT ensemble. Nosé–Hoover thermostats<sup>39</sup> were applied to the air molecules. To obtain meaningful statistics, for each set of parameters, more than 8 independent simulations were performed sufficiently long (over 8 ns). In all simulations, to substantially reduce the computational cost, all the graphene atoms were assumed to be held rigid. Further simulation details can be found in Supporting Information (SI). What's more, the time step and size effects on the ratchet transport herein are also discussed in SI.

## Results and Discussions

In each simulation, we tracked the density of air in all regions over time. A typical simulation outcome of air's density profile over time is shown in Fig. 2(a). This simulation is performed at 300 K ( $T_{amb}$ ). GTCN is constructed by 4 ( $N_l$ ) layers graphene with truncated-cone nanopores, where the area of the minimum pore is  $55.2 \text{ \AA}^2$  ( $A_{min}$ ) and the truncated-cone angle is  $\arctan 0.25$  ( $\alpha$ ). It's worth noting that different  $A_{min}$  means the area of the holes in other three graphene layers are also different. And we choose  $A_{min}$  to describe the size of truncated-cone's aperture for convenience. As shown in Fig. 2(a), we can observe a significant difference of the density about  $0.2 \text{ g/m}^3$ , between the left and right regions. This unexpected phenomenon results from the ratchet effect, producing net mass transport by rectifying thermal fluctuations.

For the sake of further enhancing the evaporation (ratchet) efficiency, we investigated the relationship between the pressure difference  $\Delta P$  with the number of graphene

layers  $N_l$ , the area of the minimum pore  $A_{min}$ , the angle of the truncated-cone  $\alpha$ , and the ambient temperature  $T_{amb}$ .

Firstly, the dependence of  $\Delta P$  on  $N_l$  was studied,  $A_{min}$  and  $\tan\alpha$  were fixed at  $33.1 \text{ \AA}^2$  and  $0.25 \text{ \AA}^2$ , respectively. As shown in Fig. 2(b), when the  $N_l$  increases from 2 to 5,  $\Delta P$  decreases linearly. To obtain the in-depth comprehension of this dependence, the force distribution (along Z axis) around GTCN was calculated by using a nitrogen atom as the probe and shown in Fig. 3. The color bar and arrows describes the magnitudes and directions of the force. Vertical axis and Horizontal axis correspond to the Y and Z axis, respectively. For better comprehension, we plot the graphene layers in this figure. A distinct symmetry breaking between the positive (rightward) and negative (leftward) force appears in the truncated-cone nanopores. According to the force distribution of GTCN with different  $N_l$ , it's clearly that the negative force (blue regions) become weaker but the positive force (red regions) remains nearly the same in the nanochannel. That's why the ratchet effect weakens with the increasing of layers.

Apart from the number of layers  $N_l$ , another important factor, the area of the minimum pore  $A_{min}$  was also discussed here. In this part, all simulations were performed at room temperature with fixed  $N_l$  (4 or 3) and  $\alpha$  ( $\arctan 0.25$ ). The results are shown in Fig. 2(c). As the  $A_{min}$  changes from  $22.1 \text{ \AA}^2$  to  $55.2 \text{ \AA}^2$ ,  $\Delta P$  increases significantly; while  $\Delta P$  sharply reduces to 3.3 KPa with  $A_{min}$  increasing to  $77.3 \text{ \AA}^2$ . The increasing tendency is consistent with the variation of force distribution along Z axis in the nanochannel (Fig. 4(b-d)), where the negative (leftward) force regions expand and the positive (rightward) force regions shrink significantly with the increasing  $A_{min}$ . However, there exists a bit weakening of negative force, which is detrimental to the ratchet transport and make the inducement of this tendency unclear. Therefore, we try to seek more interpretation by analyzing the potential distribution in the nanochannel. Because the asymmetric potential is one of the two indispensable factors for the ratchet effect. The potential of GTCN with different  $A_{min}$  and the asymmetry potential are shown in Fig. 4 (a). The potential peaks or the energy barriers locate at the position of

each graphene layer and hinder the transport of atoms. Obviously, the potential peaks of the graphene are lower for bigger holes, which means the molecules in right region get a higher probability to enter the nanochannel. Such asymmetry results in atoms flowing more easily along the convergent direction (leftward). When  $A_{min}$  increases, the nanoholes become bigger but the number and value of peaks become less and smaller. What's more, when  $A_{min}$  reach to  $55.2 \text{ \AA}^2$ , the two rightmost peaks even disappear. Consequently, compared with the weakening of negative force, the broader nanochannel and the less number and lower values of energy barriers (i.e., the potential peaks in Fig. 4(a)) are dominant, hence the strengthened ratchet effect. As for the reasons of the decreasing trend, which involves the diffusion transport, will be explained later. The other important factor, the zero-average dynamic load, is acted by thermal noise to supply the energy for continuous molecule flow. Remarkably, herein, thermal fluctuations can not be considered as white noise with negligible time correlation, because the correlation lengths of the thermal fluctuations become significantly long for nanopores<sup>40</sup>. Therefore, by absorbing heat (the power of thermal fluctuations), air molecules were pumped leftward persistently by GTCN and create the vacuum.

Similarly,  $\Delta P$  also has nonmonotonic dependence on the truncated-cone angle  $\alpha$ . In the following cases,  $N_l$  and  $A_{min}$  are fixed as 3 and  $33.1 \text{ \AA}^2$ , respectively. As shown in Fig. 2(d), we get the biggest  $\Delta P$ , 20.1 kPa, when  $\tan\alpha$  is 0.25. Figure 5 shows the force distribution of GTCN with different  $\tan\alpha$ . As for the reasons of the low  $\Delta P$  for the other three  $\alpha$ , on the one hand, the narrow nanochannel and many energy barriers of the small- $\alpha$  GTCN confine the ratchet effect; On the other hand, the strong diffusion transport (rightward) and weak negative (leftward) force of the big- $\alpha$  GTCN result in the low  $\Delta P$ . The discussions about diffusion transport are described in details below. That is why the adopted  $\tan\alpha$  of other simulations is fixed at 0.25 in this paper.

The ambient temperature is also a crucial factor, which decides the force of thermal fluctuations. If we attempt to advance the ratchet, there will be a minimum force

necessary to overcome the barriers. That is the ambient temperature should be high enough to activate the ratchet. However, if the temperature is too high (the force is too powerful), the ratchet could also run in the opposite direction. Because, compared with the power of thermal fluctuations, the asymmetric potential is so small that cannot impose the rightward movements of the air any more. Then the ratchet effect is broken. We performed the simulations with fixed  $N_l$  (4),  $A_{min}$  ( $55.2 \text{ \AA}^2$ ) and  $\tan\alpha$  (0.25) at different temperature. At the range of 300 K to 600 K, the resulting  $\Delta P$  are 20.1 kPa and 9.2 kPa, and this difference is consistent with our speculation. (details are shown in SI).

The previous discussions of results mainly focus on the strength of the ratchet effect. However, the diffusive transport, resulted from the concentration difference, also affects the molecular transport. The molecules will move from the high concentration region to the low due to the diffusive transport, and this limits the further growth of concentration. Therefore, the final distribution of air depends on the competition between the ratchet transport (leftward) and diffusive transport (rightward). Since the scale length of the truncated-cone nanopores is much smaller than the mean free path of the air molecules, the Knudsen diffusion<sup>41</sup> occurs here. The diffusion flux is defined as,

$$\Phi_k = -\frac{2}{3}\bar{r}u \frac{dC}{dz} \quad (1)$$

$$\bar{r} = (r_{min} + r_{max})/2 \quad (2)$$

$$r_{max} = r_{min} + (N_l - 1)h\tan\alpha \quad (3)$$

where  $\bar{r}$  is the mean radius of the nanochannel,  $r_{min}$  and  $r_{max}$  are radiuses of the minimum and maximum pores.  $r_{min}$  equals to  $\sqrt{A_{min}/\pi}$ ;  $u$  is the characteristic velocity of air molecules;  $\frac{dC}{dz}$  is the concentration gradient and  $h$  is the interlayer spacing of GTCN. In equation (1),  $\bar{r}$  and  $\Phi_k$  are substituted by (2)-(3). Then equation (1) can be defined as,

$$\Phi_k = -\frac{2r_{min} + (N_l - 1)h\tan\alpha}{3}u \frac{dC}{dz} \quad (4)$$



When the number of GTCN layers increases from 2 to 5,  $r_{min}$ ,  $h$  and  $\alpha$  remain the same. And the concentration of air has a negligible change,  $\frac{dC}{dz}$  is assumed to be proportional to the thickness of GTCN,  $(N_l - 1)h$ . It's clearly that Knudsen diffusion flux  $\Phi_k$  only has subtle reduction, which comes from the product of  $r_{min}$  and  $\frac{dC}{dz}$ , when  $N_l$  increases. As the consequence of the significant weakening in ratchet effect and the subtle reduction of diffusion flux,  $\Delta P$ , surely, decreases. In addition, as for the situation that  $A_{min}$  increases from  $22.1 \text{ \AA}^2$  to  $77.3 \text{ \AA}^2$ , i.e.  $r_{min}$  becomes bigger and other parameters remain the same,  $\Phi_k$  also increases according to Eq. (4). As a result, more molecules transport against the ratchet effect. However, when  $A_{min}$  increases from  $22.1 \text{ \AA}^2$  to  $55.2 \text{ \AA}^2$ , the broadening nanochannel and the decreasing of energy barriers dominate. Hence,  $\Delta P$  increases from 8.5 kPa to 15.1 kPa. But when  $A_{min}$  increase to  $77.3 \text{ \AA}^2$ , the dominant place is taken by the sustainable weakening of leftward force, which leads to the enhancement of ratchet effect becomes negligible. Thus the inflection point appears.

To illustrate its potential in practical application, the effect of GTCN on evaporation is discussed in this paragraph. The previous results and discussions provide useful guidelines for the design of GTCN. According to the results in Fig 2, GTCN can create a biggest pressure difference as 21 kPa, between the left and right region. Hence, when GTCN is used to decrease the vapor pressure near the water-vapor interface, the evaporation rate will be improved according to Hertz-Knudsen Relation<sup>42</sup> as defined here:

$$\dot{m} = \left( \sigma_e \frac{P_S}{\sqrt{T_L}} - \sigma_c \frac{P_V}{\sqrt{T_a}} \right) \sqrt{\frac{M}{2\pi R}} \quad (5)$$

where  $\dot{m}$  is the evaporation rate of the water,  $P_S$  and  $P_V$  are the water vapor saturate pressure and the real vapor partial pressure at the interface respectively.  $\sigma_e$  and  $\sigma_c$  are the evaporation and condensation coefficient respectively.  $M$  is the molar mass of the water molecule.  $T_L$  and  $T_a$  are the temperature of the water and vapor at the interface respectively.

Normally,  $\sigma_e$  and  $\sigma_c$  are measured at the range of 0.001 to 1 and very close to each other<sup>42-44</sup>.  $T_L$  is slightly higher than  $T_a$  when water is heated to evaporate.<sup>45</sup> And  $P_v$  is lower than  $P_s$  due to the lower vapor temperature and molecular diffusion to atmosphere. Therefore, the following assumptions are made:

- The temperature discontinuity at the water-vapor interface is ignored (i.e.  $T_L = T_a = T$ )
- The difference between evaporation and condensation coefficient is ignored (i.e.  $\sigma_e = \sigma_c = \varepsilon$ ).

$\eta_i$  can be described as (details are shown in SI):

$$\eta_i = \left( \frac{\varepsilon \cdot \Delta P \cdot P_s}{P_{atm} \dot{m}} \sqrt{\frac{M}{2\pi RT}} - 1 \right) \times 100\% \quad (6)$$

where  $P_{atm}$  is the atmospheric pressure,  $\Delta P$  is the pressure difference between the two sides of GTCN. It should be noted that  $\dot{m}$  is the evaporation flux without GTCN. Thus, to calculate the enhancement,  $\varepsilon$ ,  $T$ , and  $\dot{m}$  of a traditional evaporation condition (i.e. without GTCN) should be measured. Due to the lack of consensus in the value of  $\varepsilon$ , herein we regard it as an independent variable which varies from 0.001 to 1. Fig 6(a) shows the calculated enhancement according to the temperature and evaporation data from references<sup>3, 6, 45</sup>. As we can see, even if  $\varepsilon$  only equals to 0.001 in those experiments, an enhancement of 15 times can be expected at relatively low temperature. This dramatic enhancement results from the break of balance between evaporation and condensation at the interface. On the contrary, due to the diffusion resistance, macroscopic pump has slight effect on that balance. Therefore, although the considerable pressure difference can be produced, macroscopic pump still can't work well. It means, by using GTCN, a lot of low grade energy can be used for vapor generation, such as low intensity solar energy or waste heat. Meanwhile, the low evaporation temperature can decrease the energy dissipation effectively. Those merits imply a high potential of practical application of GTCN.

## Conclusion

Summarizing, based on the ratchet effect, the GTCN we proposed can pump molecules unidirectional by rectifying thermal fluctuations. By performing MD simulations, we find that GTCN can produce pressure difference as high as 21.0 kPa. It corresponds to more than 15 times enhancement compared with natural evaporation, hence it could be applied in vapor generation. We provide detailed discussions about the factors that may affect the efficiency of this nano-pump and provide guidelines for the design of multilayer membranes. It is found that the pressure difference  $\Delta P$  decreases with increasing  $N_l$ , but firstly increases and then decreases with increasing  $A_{min}$  and  $\tan\alpha$ . Moreover, we find  $\Delta P$  is not sensitive to the ambient temperature. According to the obtained results, it is better to construct GTCN by using 2 layers graphene with truncated-cone nanopores, where the area of the minimum pore is  $55.2 \text{ \AA}^2$  and the truncated-cone angle is fixed as  $\arctan 0.25$  then the best performance can be obtained. After comparatively analyzing the force and potential profile of GTCN in different conditions, we demonstrated that the ratchet transport is induced by the asymmetric potential or force in the nanochannel. Through the analysis from diffusive transport, we further demonstrated that the final distribution of air is decided by the competition between ratchet transport and diffusive transport. The results suggest that enhancement of vapor generation can be achieved by the novel multilayer graphene greenly, which is much easier to fabricate and consumes only low grade energy like low intensity solar energy and waste heat.

## **Acknowledgments**

The project was supported by the National Natural Science Foundation of China 51576076 (NY). The authors thank the National Supercomputing Center in Tianjin (NSCC-TJ) for providing help in computations. The authors are grateful to Zelin Jin, Quanwen Liao for useful discussions.

**Additional Information:** Supplementary information accompanies this paper

**Competing financial interests:** The authors declare no competing financial interests

## Reference

1. Xue, G.; Xu, Y.; Ding, T.; Li, J.; Yin, J.; Fei, W.; Cao, Y.; Yu, J.; Yuan, L.; Gong, L., Water-evaporation-induced electricity with nanostructured carbon materials. *Nature nanotechnology* **2017**.
2. Lewis, N. S., Research opportunities to advance solar energy utilization. *Science* **2016**, *351* (6271), aad1920.
3. Zhou, L.; Tan, Y.; Wang, J.; Xu, W.; Yuan, Y.; Cai, W.; Zhu, S.; Zhu, J., 3D self-assembly of aluminium nanoparticles for plasmon-enhanced solar desalination. *Nature Photonics* **2016**, *10* (6), 393-398.
4. Shannon, M. A.; Bohn, P. W.; Elimelech, M.; Georgiadis, J. G.; Marinas, B. J.; Mayes, A. M., Science and technology for water purification in the coming decades. *Nature* **2008**, *452* (7185), 301-10.
5. Absi Halabi, M.; Al-Qattan, A.; Al-Otaibi, A., Application of solar energy in the oil industry—Current status and future prospects. *Renewable and Sustainable Energy Reviews* **2015**, *43*, 296-314.
6. Ghasemi, H.; Ni, G.; Marconnet, A. M.; Loomis, J.; Yerci, S.; Miljkovic, N.; Chen, G., Solar steam generation by heat localization. *Nature communications* **2014**, *5*, 4449.
7. Ni, G.; Li, G.; Boriskina, Svetlana V.; Li, H.; Yang, W.; Zhang, T.; Chen, G., Steam generation under one sun enabled by a floating structure with thermal concentration. *Nature Energy* **2016**, *1* (9), 16126.
8. Neumann, O.; Urban, A. S.; Day, J.; Lal, S.; Nordlander, P.; Halas, N. J., Solar Vapor Generation Enabled by Nanoparticles. *Acs Nano* **2013**, *7* (1), 42-9.
9. Fang, Z.; Zhen, Y. R.; Neumann, O.; Polman, A.; Garcia de Abajo, F. J.; Nordlander, P.; Halas, N. J., Evolution of light-induced vapor generation at a liquid-immersed metallic nanoparticle. *Nano letters* **2013**, *13* (4), 1736-42.
10. Ranjan, R.; Murthy, J. Y.; Garimella, S. V., A microscale model for thin-film evaporation in capillary wick structures. *International Journal of Heat & Mass Transfer* **2011**, *54* (1-3), 169-179.
11. Nassar, Y. F.; Yousif, S. A.; Salem, A. A., The second generation of the solar desalination systems. *Desalination* **2007**, *209* (1-3), 177-181.
12. Kabeel, A. E.; Omara, Z. M.; Essa, F. A., Enhancement of modified solar still integrated with external condenser using nanofluids: An experimental approach. *Energy Conversion and Management* **2014**, *78*, 493-498.
13. Hänggi, P.; Marchesoni, F., Artificial Brownian motors: Controlling transport on the nanoscale. *Reviews of Modern Physics* **2009**, *81* (1), 387-442.
14. Smoluchowski, M., Experimentell nachweisbare, der üblichen Thermodynamik widersprechende Molekularphänomene. *Pisma Mariana Smoluchowskiego* **1927**, *2* (1), 226-251.
15. Mochizuki, M.; Yu, X. Z.; Seki, S.; Kanazawa, N.; Koshibae, W.; Zang, J.; Mostovoy, M.; Tokura, Y.; Nagaosa, N., Thermally driven ratchet motion of a skyrmion microcrystal and topological magnon Hall effect. *Nature materials* **2014**, *13* (3), 241-6.
16. Longhurst, M.; Quirke, N., Temperature-driven pumping of fluid through single-walled carbon nanotubes. *Nano letters* **2007**, *7* (11), 3324-3328.
17. Lavrijsen, R.; Lee, J. H.; Fernandez-Pacheco, A.; Petit, D. C.; Mansell, R.; Cowburn, R. P., Magnetic ratchet for three-dimensional spintronic memory and logic. *Nature* **2013**, *493* (7434), 647-50.
18. Takano, M.; Terada, T. P.; Sasai, M., Unidirectional Brownian motion observed in an in silico single molecule experiment of an actomyosin motor. *Proc Natl Acad Sci U S A* **2010**, *107* (17), 7769-74.
19. Drexler, C.; Tarasenko, S. A.; Olbrich, P.; Karch, J.; Hirmer, M.; Muller, F.; Gmitra, M.; Fabian, J.; Yakimova, R.; Lara-Avila, S.; Kubatkin, S.; Wang, M.; Vajtai, R.; Ajayan, P. M.; Kono, J.; Ganichev, S. D.,

- Magnetic quantum ratchet effect in graphene. *Nature nanotechnology* **2013**, *8* (2), 104-7.
20. Gong, X.; Li, J.; Lu, H.; Wan, R.; Li, J.; Hu, J.; Fang, H., A charge-driven molecular water pump. *Nature nanotechnology* **2007**, *2* (11), 709-12.
  21. Chinappi, M.; De Angelis, E.; Melchionna, S.; Casciola, C. M.; Succi, S.; Piva, R., Molecular Dynamics Simulation of Ratchet Motion in an Asymmetric Nanochannel. *Physical Review Letters* **2006**, *97* (14).
  22. Guo, P.; Zheng, Y.; Wen, M.; Song, C.; Lin, Y.; Jiang, L., Icephobic/anti-icing properties of micro/nanostructured surfaces. *Adv Mater* **2012**, *24* (19), 2642-8.
  23. Guo, P.; Wen, M.; Wang, L.; Zheng, Y., Strong anti-ice ability of nanohairs over micro-ratchet structures. *Nanoscale* **2014**, *6* (8), 3917-20.
  24. Rozhansky, I. V.; Kachorovskii, V. Y.; Shur, M. S., Helicity-Driven Ratchet Effect Enhanced by Plasmons. *Phys Rev Lett* **2015**, *114* (24), 246601.
  25. Doering, C. R.; Horsthemke, W.; Riordan, J., Nonequilibrium fluctuation-induced transport. *Physical review letters* **1994**, *72* (19), 2984.
  26. Van den Broeck, C.; Kawai, R.; Meurs, P., Microscopic analysis of a thermal brownian motor. *Phys Rev Lett* **2004**, *93* (9), 090601.
  27. Roche, B.; Roulleau, P.; Jullien, T.; Jompol, Y.; Farrer, I.; Ritchie, D. A.; Glattli, D. C., Harvesting dissipated energy with a mesoscopic ratchet. *Nature communications* **2015**, *6*, 6738.
  28. Hummer, G.; Rasaiah, J. C.; Noworyta, J. P., Water conduction through the hydrophobic channel of a carbon nanotube. *Nature* **2001**, *414* (6860), 188-190.
  29. Joseph, S.; Aluru, N., Why are carbon nanotubes fast transporters of water? *Nano letters* **2008**, *8* (2), 452-458.
  30. Majumder, M.; Chopra, N.; Andrews, R.; Hinds, B. J., Nanoscale hydrodynamics: enhanced flow in carbon nanotubes. *Nature* **2005**, *438* (7064), 44-44.
  31. Holt, J. K.; Park, H. G.; Wang, Y.; Stadermann, M.; Artyukhin, A. B.; Grigoropoulos, C. P.; Noy, A.; Bakajin, O., Fast mass transport through sub-2-nanometer carbon nanotubes. *Science* **2006**, *312* (5776), 1034-1037.
  32. Rasaiah, J. C.; Garde, S.; Hummer, G., Water in nonpolar confinement: From nanotubes to proteins and beyond\*. *Annu. Rev. Phys. Chem.* **2008**, *59*, 713-740.
  33. Radha, B.; Esfandiari, A.; Wang, F. C.; Rooney, A. P.; Gopinadhan, K.; Keerthi, A.; Mishchenko, A.; Janardanan, A.; Blake, P.; Fumagalli, L.; Lozada-Hidalgo, M.; Garaj, S.; Haigh, S. J.; Grigorieva, I. V.; Wu, H. A.; Geim, A. K., Molecular transport through capillaries made with atomic-scale precision. *Nature* **2016**, *538* (7624), 222-225.
  34. Plimpton, S., Fast parallel algorithms for short-range molecular dynamics. *Journal of Computational Physics* **1995**, *117* (1), 1-19.
  35. Ohba, T., The thinnest molecular separation sheet by graphene gates of single-walled carbon nanohorns. **2014**, *8* (11), 11313-9.
  36. Abascal, J. L. F., A general purpose model for the condensed phases of water: TIP4P/2005. *Journal of Chemical Physics* **2005**, *123* (23), 234505-234505-12.
  37. Beu, T. A., Molecular dynamics simulations of ion transport through carbon nanotubes. I. Influence of geometry, ion specificity, and many-body interactions. *The Journal of chemical physics* **2010**, *132* (16), 164513.
  38. Ma, D.; Ding, H.; Wang, X.; Yang, N.; Zhang, X., The unexpected thermal conductivity from graphene disk, carbon nanocone to carbon nanotube. *International Journal of Heat and Mass Transfer* **2017**, *108*, 940-944.

39. Martyna, G. J.; Klein, M. L.; Tuckerman, M., Nose-Hoover chains: the canonical ensemble via continuous dynamics. *J Chem Phys* 97:2635. *Journal of Chemical Physics* **1992**, 97 (4), 2635-2643.
40. Wan, R.; Hu, J.; Fang, H., Asymmetric transportation induced by thermal noise at the nanoscale. *Science China Physics, Mechanics and Astronomy* **2012**, 55 (5), 751-756.
41. Knudsen; Martin, Die Gesetze der Molekularströmung und der inneren Reibungsströmung der Gase durch Röhren. *Annalen Der Physik* **1909**, 333 (1), 75-130.
42. Persad, A. H.; Ward, C. A., Expressions for the Evaporation and Condensation Coefficients in the Hertz-Knudsen Relation. *Chem Rev* **2016**, 116 (14), 7727-67.
43. Eames, I. W.; Marr, N. J.; Sabir, H., The evaporation coefficient of water: a review. *International Journal of Heat & Mass Transfer* **2013**, 40 (12), 2963-2973.
44. Marek, R.; Straub, J., Analysis of the evaporation coefficient and the condensation coefficient of water. *International Journal of Heat & Mass Transfer* **2001**, 44 (1), 39-53.
45. Li, Y.; Xia, G.; Jia, Y.; Cheng, Y.; Wang, J., Experimental investigation of flow boiling performance in microchannels with and without triangular cavities – A comparative study. *International Journal of Heat & Mass Transfer* **2017**, 108, 1511-1526.

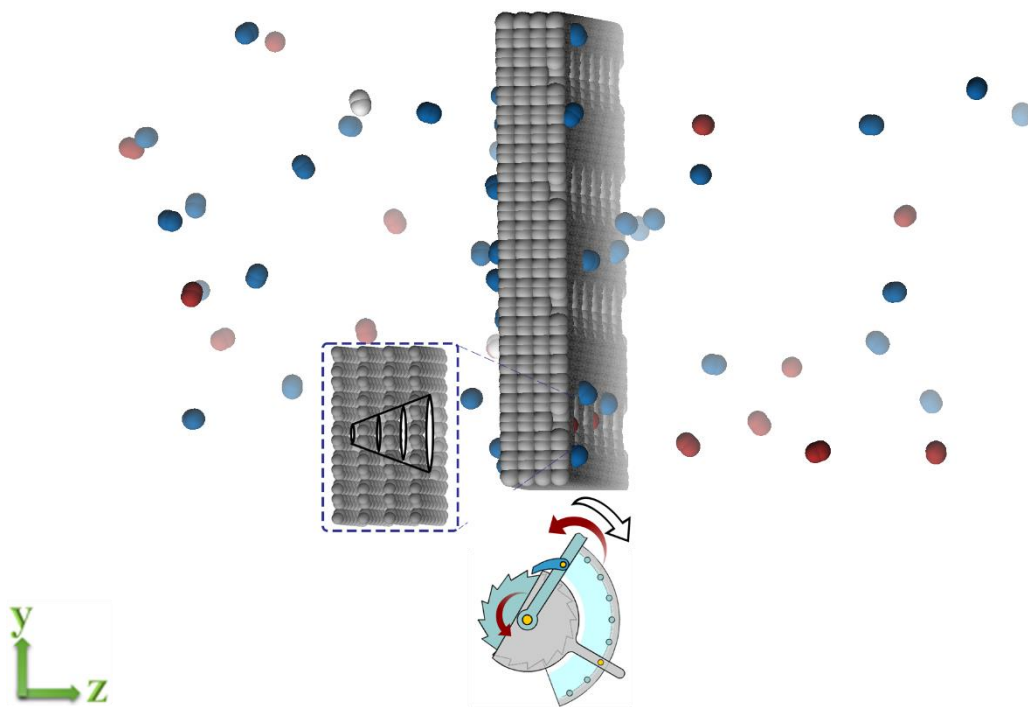


Figure 1. Schematic graph for the simulation setup. Multilayer graphene membranes with truncated-cone nanopores are in grey; Nitrogen, oxygen and hydrogen molecules are in blue, red and white, respectively. The thermal fluctuations act as the rod, running back and forth. The GTCN acts as the pawl and rectify the work of the rod. Then the rotary direction of the gear is clockwise. That is the transport direction of the air atoms is leftward. The two arrows around the rod shows the directions of thermal fluctuations' work. And the arrow around the gear shows the direction of the ratchet transport.

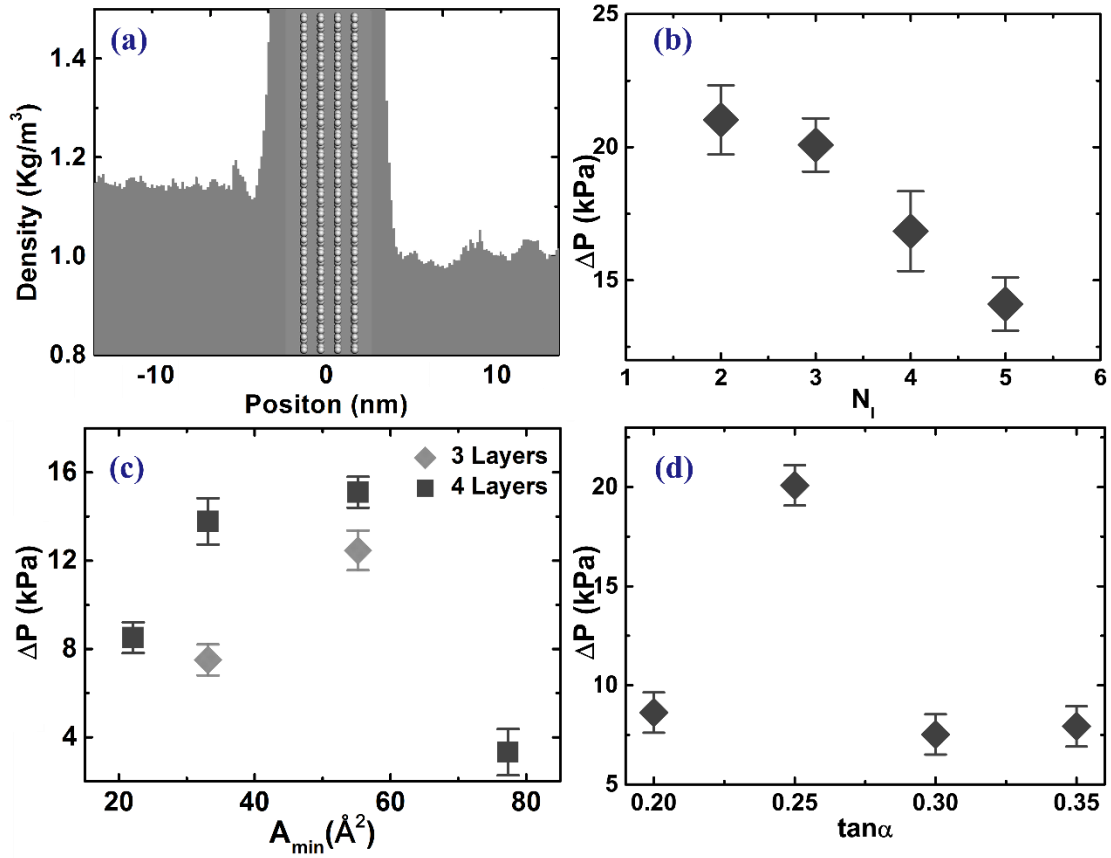


Figure 2. (a) A typical density profile of saturated moist air molecules. In this simulation, GTCN is constructed by 4 layers graphene with truncated cone nanopores, where the area of minimum pore is  $55.2 \text{ \AA}^2$  and the angle of the truncated-cone  $\alpha$  is 0.25. The dependence of the pressure difference  $\Delta P$  on the number of graphene layers  $N_l$  (b), the minimum pore's area  $A_{min}$  (c) and the angle of the truncated-cone  $\alpha$  (d).



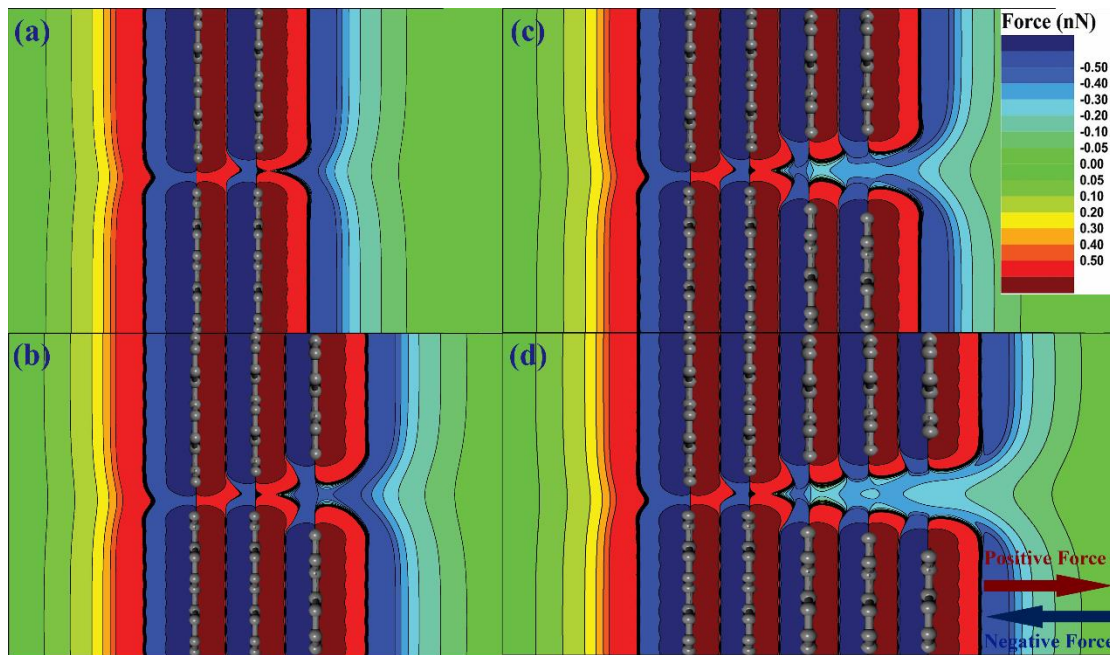


Figure 3. The force (along the Z direction) distribution of GTCN with different graphene layers (from 2 layers to 5 layers). The area of minimum pore is fixed as  $33.1 \text{ \AA}^2$  and the angle of the truncated-cone  $\alpha$  as 0.25. The arrows point out the direction of positive and negative forces.

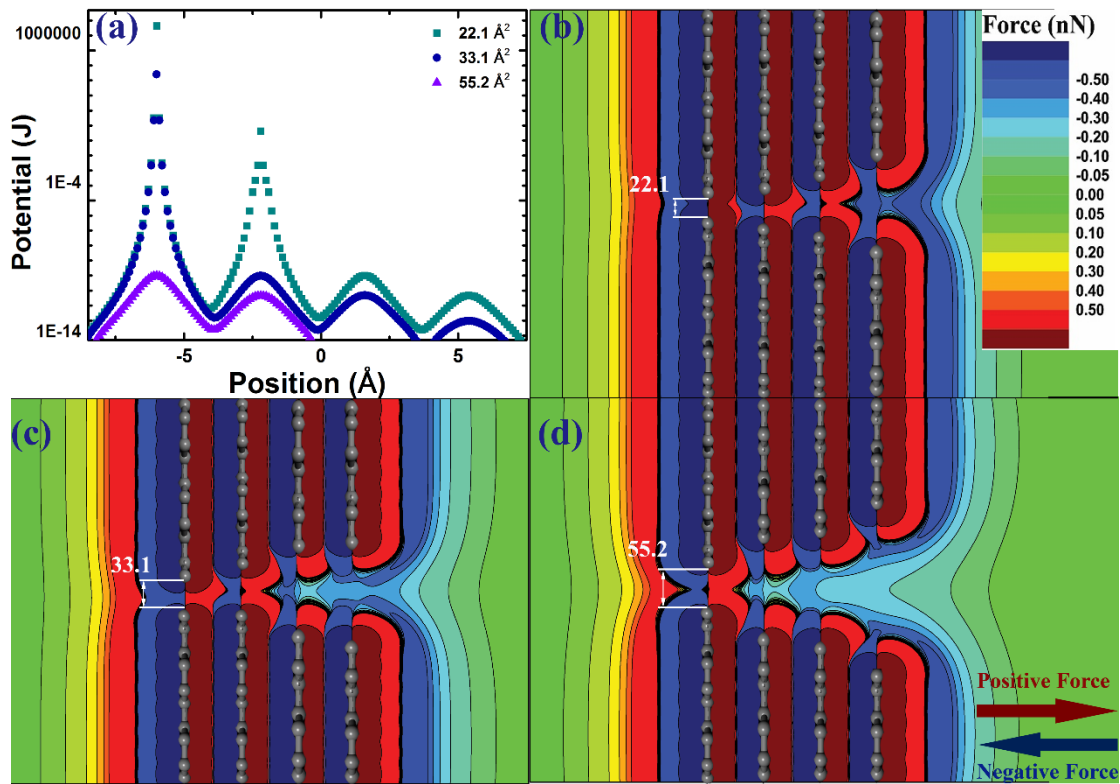


Figure 4. The potential (a) and the force (along the Z direction) (b)-(c) profile of the GTCN with different  $A_{min}$  (from 22.1 Å<sup>2</sup> to 55.2 Å<sup>2</sup>) are shown in. The number of GTCN layers is fixed as 4 and the angle of the truncated-cone  $\alpha$  as 0.25. The arrows point out the direction of positive and negative force.

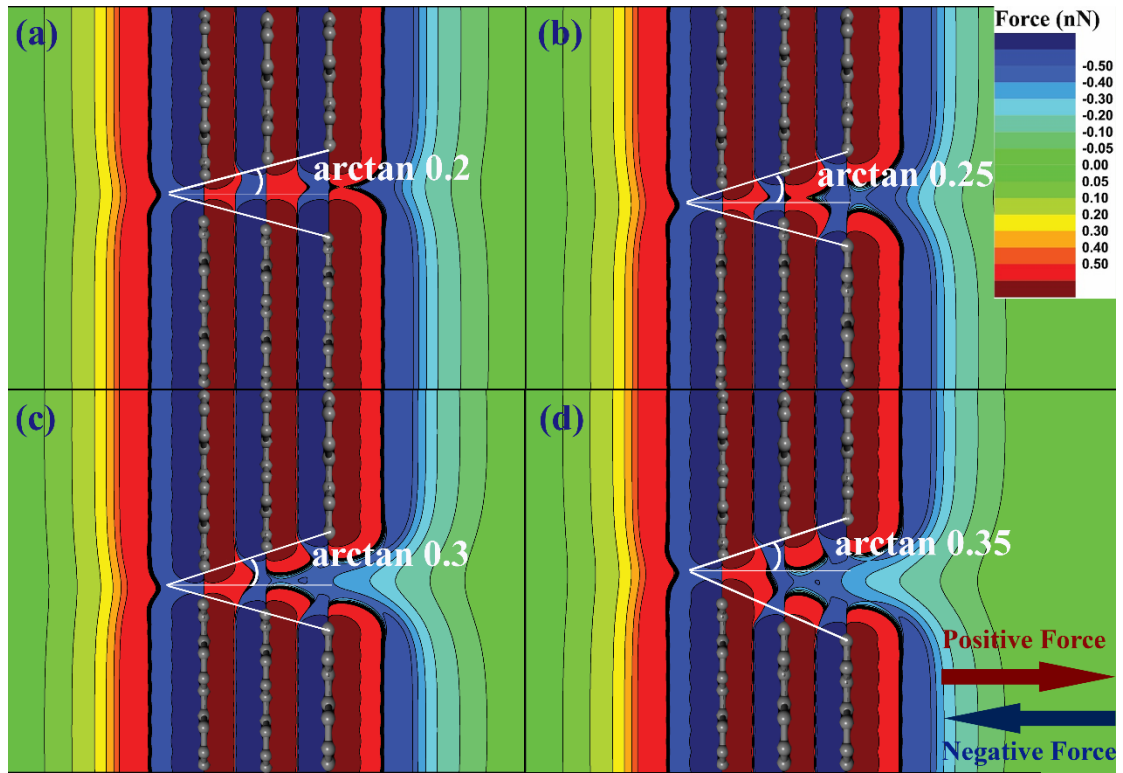


Figure 5. The number of GTCN layers is fixed as 3; and the area of minimum pore  $A_m$  as  $33.1 \text{ \AA}^2$ . The force (along the Z direction) distribution of GTCN with different tangent of the truncated-cone angle  $\tan\alpha$  (0.2-0.35) are shown in (a)-(d). The arrows point out the direction of positive and negative force.

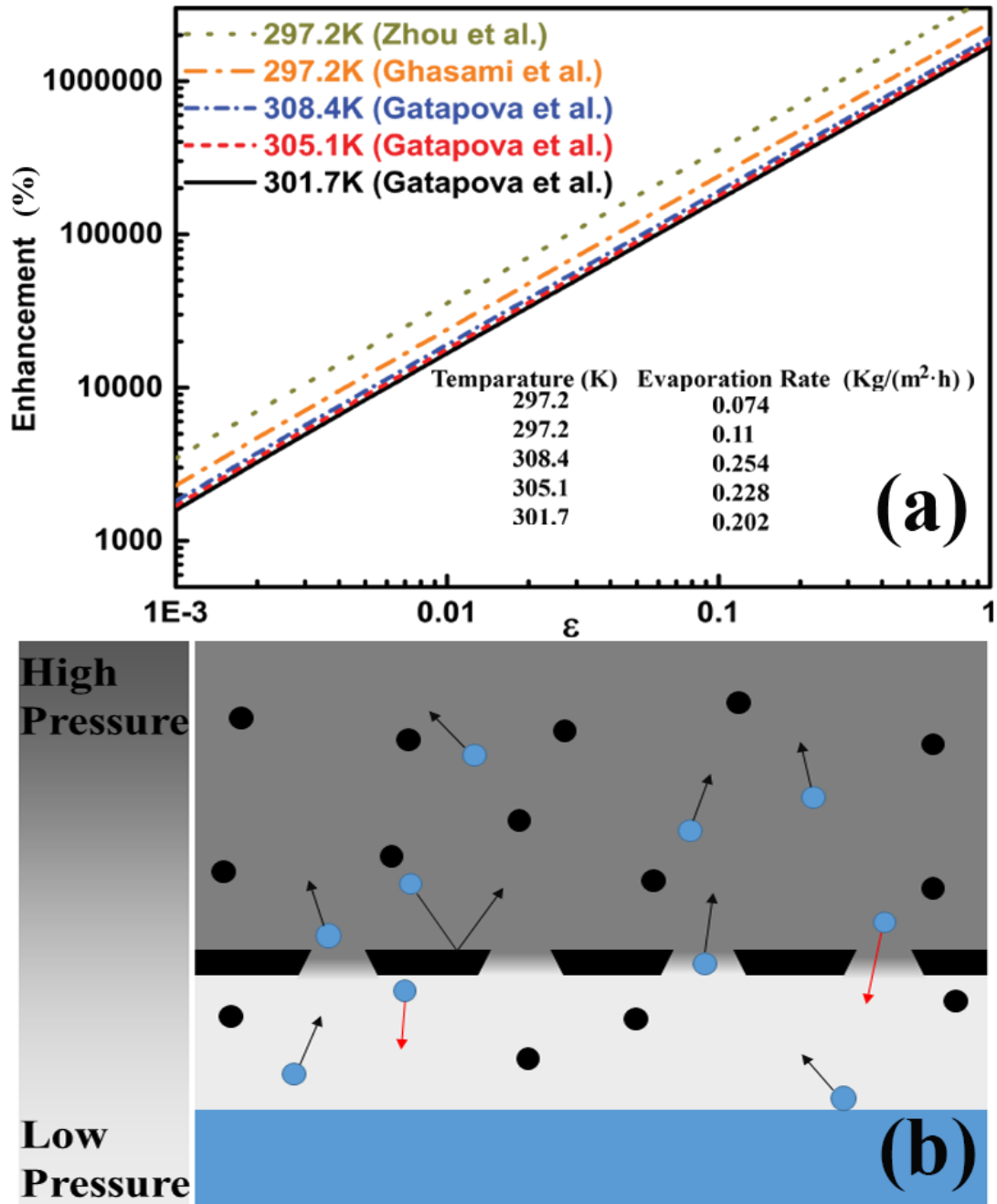


Figure 6. (a) The enhancement of evaporation at different water temperature. (b) Schematic graph for the evaporation with GTCN.

Supporting Information

**Ratchet Effect on Gas Transport by Nanoporous Graphene  
- Significant Enhancement of Vapor Generation**

Hongru Ding<sup>1,2,#</sup>, Guilong Peng<sup>1,2,#</sup>, Dengke Ma<sup>1,2</sup>, S.W. Sharshir<sup>1,2</sup> and  
Nuo Yang<sup>1,2,\*</sup>

<sup>1</sup>State Key Laboratory of Coal Combustion, Huazhong University of Science and  
Technology (HUST), Wuhan 430074, P. R. China

<sup>2</sup>Nano Interface Center for Energy(NICE), School of Energy and Power Engineering,  
Huazhong University of Science and Technology (HUST), Wuhan 430074, P. R. China

# H. D. and G. P. contributed equally to this work.

Electronic mail: N.Y. ([nuo@hust.edu.cn](mailto:nuo@hust.edu.cn))

## SI. Molecular dynamic simulation details

<b>Method</b>	Non- Equilibrium MD						
<b>Potential</b>							
<b>Function</b>	$E = \sum_i^{on\ a} \sum_j^{on\ b} \frac{k_c q_i q_j}{r_{ij}} + \frac{A}{r_{oo}^{12}} - \frac{B}{r_{oo}^6} + 4\epsilon \left[ \left( \frac{\sigma}{r} \right)^{12} - \left( \frac{\sigma}{r} \right)^6 \right]$						
<b>Parameters (TIP4P)</b>	m <sub>O</sub>	m <sub>H</sub>	q <sub>M</sub> (C)	q <sub>H</sub> (C)	R <sub>OM</sub> (Å)	R <sub>coul,cut</sub> (Å)	
	15.999	1.008	-1.040	0.520	0.15	8.5	
	R <sub>OH</sub> (Å)	θ <sub>OH</sub> (°)	A × 10 <sup>-3</sup> (Kcal Å <sup>12</sup> /(mol))		B (Kcal Å <sup>6</sup> /(mol))		
	0.9572	104.52	600.0		610.0		
<b>Parameters (VDW)</b>	Type of molecular	N <sub>2</sub> *	O <sub>2</sub> *	C	*Two centered LJ potential for N <sub>2</sub> and O <sub>2</sub>		
	ε (Kcal/(mol*Å <sup>2</sup> ))	0.0725	0.1034	0.05528			
	Σ (Å)	3.32	2.99	3.415			
<b>Simulation process</b>							
<b>Ensemble</b>	<b>Setting</b>					<b>Purpose</b>	
NVT	Time step (fs)	1	Runtime (ns)	3		Relax structure	
	Temperature (K)	300	Thermostat	Nosé–Hoover			
	Simulation cell (nm)	13.6*12.2*22					
	Boundary condition	X, Y, Z: periodic, periodic, fixed					
NVT	Runtime (ns)	8	Temperature (K)	300		Record information	
	Simulation cell (nm)	13.6*12.2*22					
	Boundary condition	X, Y, Z: periodic, periodic, fixed					

## SII. Test of timestep

In molecular dynamic simulations, the timestep size is constrained by the demand that the vibrational motion of the atoms be accurately tracked. Usually, timestep is limited to femtosecond scale<sup>34</sup>. To perform accurate but economic simulations, we made a test about different timesteps. We fix  $N_l$ ,  $A_{min}$  and  $\tan\alpha$  as 3,  $33.1\text{\AA}^2$  and 0.25, in this part. we calculate the pressure difference of GTCN with different timesteps at room temperature, the results are shown in Fig S1. The values of  $\Delta P$  change little when the timesteps are smaller than 1 fs. It shows that our simulation cell is large enough to overcome the finite size effect on calculating thermal conductivity. In all of the simulations of GTCN, we use 1 fs as the timestep.

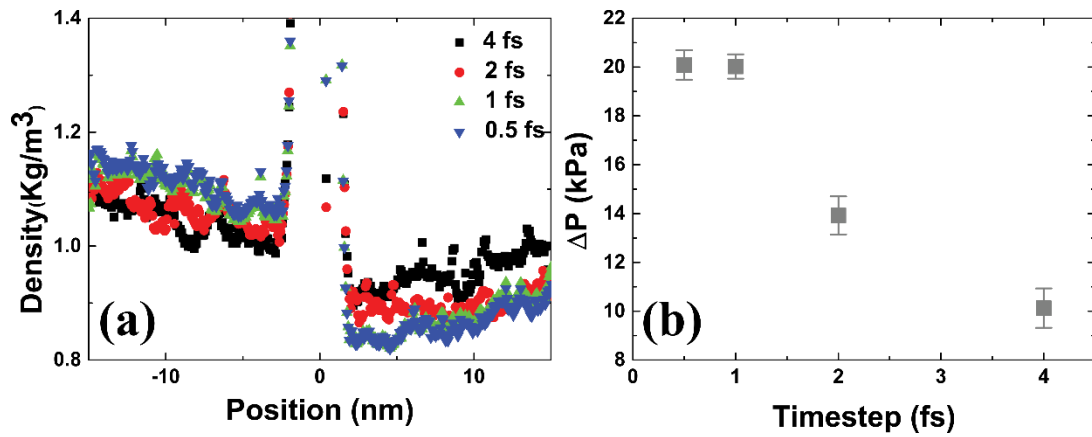


Figure S1. The density profile of saturated moist air molecules (a) and the pressure difference (b) with different timesteps. In this simulation, GTCN is constructed by 3 layers graphene with truncated cone nanopores. The area of minimum pore is  $33.1\text{\AA}^2$  and the angle of the truncated-cone  $\alpha$  is 0.25.

### SIII. Finite size effect

In this simulation, the finite size effect could arise if the simulation cell is not sufficiently large. As shown in Figure S2, we calculate the pressure difference  $\Delta P$  of GTCN with different sizes at room temperature. We fix the number of graphene layers  $N_l$ , the area of the minimum pore  $A_{min}$  and the angle of the truncated-cone  $\alpha$  as 2,  $33.1\text{\AA}^2$  and  $\arctan 0.25$ , respectively. The values of  $\Delta P$  change little when the size of simulation cell is larger than  $4\times 4$  unit cells (UCs). It shows that our simulation cell is large enough to overcome the finite size effect on calculating ratchet transport. In all of the simulations of GTCN, we use  $4\times 6$  UCs as simulation cell.

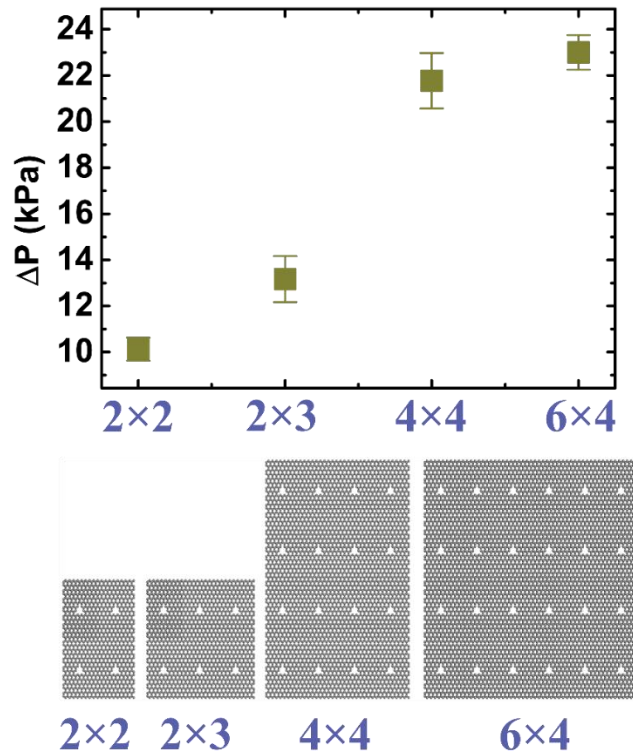


Figure S2. The pressure difference versus simulation cells. In this simulation, GTCN is constructed by 2 layers graphene with truncated cone nanopores, where the area of minimum pore is  $33.1\text{\AA}^2$  and the angle of the truncated-cone  $\alpha$  is 0.25.



#### SIV. Dependence of ambient temperature

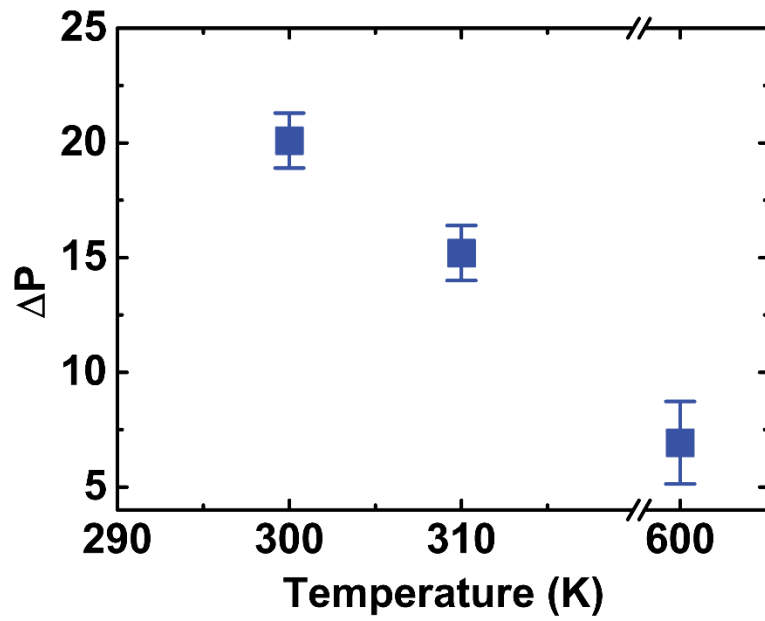


Figure S3. The pressure difference versus ambient temperature.  $\Delta P$  shows a significant reduction, when ambient temperature increase from 300 K to 600 K. In this simulation, GTCN is constructed by 4 layers graphene with truncated cone nanopores, where the area of minimum pore is  $55.2 \text{ \AA}^2$  and the angle of the truncated-cone  $\alpha$  is 0.25.

## SV. Evaporation enhancement calculation

According to Hertz-Knudsen Relation [Chemical Reviews, 2016, 116(14): 7727-7767] as defined here:

$$\dot{m} = \left( \sigma_e \frac{P_S}{\sqrt{T_L}} - \sigma_c \frac{P_V}{\sqrt{T_a}} \right) \sqrt{\frac{M}{2\pi R}} \quad (1)$$

when GTCN is applied, the enhancement of evaporation,  $\eta_i$ , can be calculated as:

$$\eta_i = \frac{P_V - P'_V}{(P_S - P_V)} \times 100\% \quad (2)$$

where  $P'_V$  and  $P_V$  are the real vapor saturate pressure at the interface with and without GTCN respectively. According to equation (1),  $P_V$  can be described as:

$$P_V = P_S - \frac{\dot{m}}{\varepsilon} \sqrt{\frac{2\pi RT}{M}} \quad (3)$$

Meanwhile, as shown in Figure S4, due to the diffusion resistance, the vapor would accumulate on the high pressure side, which indicates that the pressure on the high pressure side of GTCN can be regarded as  $P_S$ . Therefore,  $P'_V$  can be determined by:

$$P'_V = \left( 1 - \frac{\Delta P}{P_{atm}} \right) P_S \quad (4)$$

where  $P_{atm}$  is the atmospheric pressure,  $\Delta P$  is the pressure difference between the two sides of GTCN. Hence,  $\eta_i$  can be described as:

$$\eta_i = \left( \frac{\varepsilon \cdot \Delta P \cdot P_S}{P_{atm} \dot{m}} \sqrt{\frac{M}{2\pi RT}} - 1 \right) \times 100\% \quad (5)$$

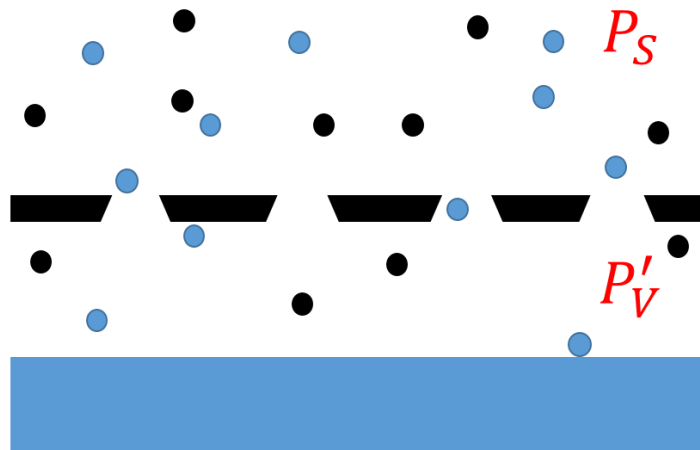


Figure S4 Vapor pressure on both sides of GTCN. The pressure at the interface,  $P'_V$ , is low due to the pumping by GTCN, the pressure on the other side is  $P_S$  due to the accumulation of vapor molecules.